drinking water. On the basis of the volume of ZnS precipitated in the biofilm, we estimate that the biofilm has concentrated Zn at least 10^6 times relative to the bulk fluid.

There is considerable controversy associated with interpretation of the complex paragenetic sequences responsible for Zn ore deposit formation. Organic geochemical and isotopic indicators of biological sulfate reduction have been reported from some Pb and Zn deposits (*21*, *22*), and microbial precipitation of metastable iron sulfides in sediments is widely accepted. The precipitation process we document is expected to operate under a fairly wide range of temperature conditions and could readily generate mixed metal sulfide assemblages [including galena (PbS) at an Eh of −130 mV in (*8*)] if heterogeneities in sulfide concentration (and thus, Eh) develop (Fig. 6). The process may be relevant to the early stages of formation of the large sediment-hosted deposits from brines, exhalative fluids, or basinal fluids, and to formation of other low-temperature ZnS deposits.

References and Notes

1. M. Ledin, K. Pedersen, *Earth-Sci. Rev.* **41**, 67 (1996).
2. H. L. Ehrlich, *Geomicrobiol. J.* **16**, 135 (1999).
3. L. P. Miller, *Boyce Thompson Inst. Contr.* **16**, 85 (1950).
4. L. G. M. Baas Becking, D. Moore, *Econ. Geol.* **56**, 259 (1961).
5. K. L. Temple, N. LeRoux, *Econ. Geol.* **59**, 647 (1964).
6. W. J. Drury, *Water Environ. Res.* **71**, 1244 (1999).
7. U.S. Environmental Protection Agency, Office of Ground Water and Drinking Water, *Current Drinking Water Standards* (2000).
8. Supplementary data are available at *Science* Online at www.sciencemag.org/cgi/content/full/290/5497/1744/DC1.
9. J. F. Banfield, S. A. Welch, H. Zhang, T. T. Ebert, R. L. Penn, *Science* **289**, 751 (2000).
10. G. W. Luther III, A. L. Meyerson, J. J. Krajewski, R. Hires, *J. Sediment. Petrol.* **50**, 1117 (1980).
11. E. T. Degens, H. Okada, S. Honjo, J. C. Hathaway, *Mineral. Deposita* **7**, 1 (1972).
12. D. K. Newman, D. Ahmann, F. M. M. Morel, *Geomicrobiol. J.* **15**, 255 (1998).
13. D. C. Nelson *et al.*, *Geochem. Cosmochim. Acta.* **60**, 3531 (1996).
14. M. Vainshtein, H. Hippe, R. M. Kroppenstedt, *Syst. Appl. Microbiol.* **15**, 554 (1992).
15. F. Widdel, F. Bak, in *The Prokaryotes*, A. Balows, H. G. Trüper, M. Dworkin, W. Harder, K.-H. Schleifer, Eds. (Springer-Verlag, New York, 1992), pp. 3352–3378.
16. D. Minz *et al.*, *Appl. Environ. Microbiol.* **65**, 4659 (1999).
17. D. Minz *et al.*, *Appl. Environ. Microbiol.* **65**, 4666 (1999).
18. A. Teske *et al.*, *Appl. Environ. Microbiol.* **64**, 2943 (1998).
19. L. G. Benning, R. T. Wilkin, H. L. Barnes, *Chem. Geol.* **167**, 25 (2000).
20. SRB were enriched in modified DSMZ 63-media (DSMZ, Braunschweig, Germany); instead of lactate, pyruvate was used as carbon source, and $FeSO_4$ or $ZnSO_4$ was used as electron acceptor. Subsequently, 10 ml of the $FeSO_4$ media were combined with 50 ml of $ZnSO_4$ media and inoculated with 300 μl of homogenized white biofilm. Incubation occurred anaerobically at ~19°C.
21. M. A. Hu, J. R. Disnar, L. Barbanson, I. Suarez-Ruiz, *Can. J. Earth Sci.* **35**, 936 (1998).
22. G. A. Logan, M. C. Hinman, M. R. Walter, R. E. Summons, *Geochem. Cosmochim. Acta*, in press (2000).
23. W. H. Casey, P. E. Brown, B. F. Jones, S. Golding, and H. L. Ehrlich provided constructive comments. We thank P. Taglia for BTEX analyses; W. W. Barker for sample preparation; K. Meverden, A. Gesell, G. Gormann, R. Polich, and R. Clark for assistance with sampling; and K. W. Germino, J. Maser, Z. Cai, and P. Ilinski for assistance with the x-ray microprobe experiment. Banfield's group acknowledges financial support from the U.S. Department of Energy (DOE) Office of Basic Energy Sciences, NSF Division of Earth Sciences Programs, and the NASA Jet Propulsion Laboratory Astrobiology Institute. The x-ray microprobe analyses carried out at the Advanced Photon Source were supported by the DOE Office of Energy Research, Office of Basic Energy Sciences, and Office of Biological and Environmental Research (NABIR Program) and internal Argonne National Laboratory (LDRD) funds. Support for PEEMS analysis was provided by the Ecole Polytechnique Federale de Lausanne, the Swiss Fonds National de la Recherche Scientifique, and the University of Wisconsin Synchrotron Radiation Center. Electron microscopy was carried out in the Materials Science Center, University of Wisconsin–Madison. G.A.L. and R.E.S. publish with permission of the chief executive of the Australian Geological Survey Organization.

7 August 2000; accepted 6 October 2000

Tropical Climate at the Last Glacial Maximum Inferred from Glacier Mass-Balance Modeling

Steven W. Hostetler[1] and Peter U. Clark[2]

Model-derived equilibrium line altitudes (ELAs) of former tropical glaciers support arguments, based on other paleoclimate data, for both the magnitude and spatial pattern of terrestrial cooling in the tropics at the last glacial maximum (LGM). Relative to the present, LGM ELAs were maintained by air temperatures that were 3.5° to 6.6°C lower and precipitation that ranged from 63% wetter in Hawaii to 25% drier on Mt. Kenya, Africa. Our results imply the need for a ~3°C cooling of LGM sea surface temperatures in the western Pacific warm pool. Sensitivity tests suggest that LGM ELAs could have persisted until 16,000 years before the present in the Peruvian Andes and on Papua, New Guinea.

Fossil pollen and the geologic record showing an ~900-m lowering of equilibrium line altitudes (ELAs) of former tropical glaciers (*1*) have long been used to argue that tropical sea surface temperatures (SSTs) were lower during the last glacial maximum (LGM, 21,000 years ago) than those reconstructed by Climate/Long-Range Investigation, Mapping and Prediction (CLIMAP) project members (*2–6*). Because upper treeline records are possibly compromised by the effects of lower atmospheric CO_2 concentrations at the LGM (*7*), former glaciers are the principal source of high-altitude paleoclimate data in the tropics. Traditionally, paleotemperatures inferred from glacial records have been based on the assumption that lower ELAs were solely the result of temperature changes associated with modern atmospheric lapse rates. Quantifying LGM temperatures that supported lower ELAs on tropical glaciers is complicated, however, by the relative contributions of precipitation (and perhaps net radiation) that also influence the ELA. Moreover, recent analyses of low- and mid-altitude pollen records suggest that tropical atmospheric lapse rates during the LGM may have differed from those of present (*5*), and so the possibility exists that temperature anomalies may have varied with elevation. Uncertainties in the age of maximum ELA depression further complicate inferences of LGM climate made from glacial records (*8–11*).

Here we apply a mass-balance model to several key tropical glaciers to determine the LGM temperature and precipitation climatologies required to produce glaciers in mass balance with surface areas that match those estimated from the geologic record. Baseline LGM temperature and precipitation values used in the glacier model were obtained from simulations conducted with the GENESIS (v. 2.01) atmospheric general circulation model (AGCM). Three multiyear simulations are considered: a present-day simulation with fixed SSTs (control), an LGM simulation in which the CLIMAP SST reconstruction is specified (CLIMAP), and an LGM simulation with an SST field in which lower tropical SSTs than those of CLIMAP are prescribed in the eastern tropical Pacific and equatorial Atlantic Oceans [Oregon State University (OSU)] (*12, 13*). Other than SSTs, the GENESIS simulations were run with standard prescribed boundary conditions (*14*).

Monthly average values of temperature and precipitation from GENESIS were interpolated (*15*) onto a high-resolution (1-km) digital elevation model (DEM) (*16*) that resolves most, but not all, of the topographic

[1]U.S. Geological Survey, Department of Geosciences, Oregon State University, Corvallis, OR 97331, USA. E-mail: steve@ucar.edu. [2]Department of Geosciences, Oregon State University, Corvallis, OR 97331, USA. E-mail: clarkp@ucs.orst.edu

features that influence glacier morphology. Air temperatures at the targeted elevation grids were obtained from the vertical levels of GENESIS; use of the modeled vertical temperature structure of the free atmosphere from the AGCM avoids the need to specify glacial-to-interglacial changes in temperature lapse rates (*5*, *6*). Precipitation at each grid point is either the baseline GENESIS value or the GENESIS value modified to reflect the altitudinal dependence of precipitation in the tropics.

The high-resolution climate data provide input for a positive degree-day (PDD) model, a type of model that is widely applied to model the mass balance of ice sheets and glaciers (*17*–*19*). The PDD model is used to compute the water-equivalent volumes of accumulation and ablation (that is, the mass balance) at each DEM grid point (*20*). The model determines glacier area by integrating the mass balance of the individual grid points so that net mass balance equals zero. For the LGM, we use the geologic record of glacier area as the constraint for modeled area. Where necessary, we adjust the baseline GENESIS air temperature to produce a modeled area that matches the geologic target area. The baseline GENESIS precipitation values were not perturbed. From the modeled glaciers, we reconstruct the vertical gradient of mass balance from which we identify the ELA. The model does not incorporate glacier flow dynamics.

The computed ELAs and mass-balance gradients of modern glaciers on Irian Jaya, Mt. Kenya, and Mt. Kilimanjaro and ELAs in the Peruvian Andes are comparable to observations (Figs. 1 and 2). Differences that exist between computed and observed features in part reflect limitations of GENESIS and the PDD model in resolving the regional and local topographic influences on climate (such as mesoscale circulations and radiation) and glacier morphology that influence the mass balance of the modern small tropical glaciers. Although we successfully simulate both the ELA and the vertical gradient of mass balance of present-day glaciers on Irian Jaya and Mt. Kenya (Fig. 1), the simulated areas of the glaciers are larger (by up to 50%) than observed. These glaciers, like others in the tropics (*21*–*24*), have been receding rapidly over the past century (*25*) and occupy narrow steep valleys that provide favorable conditions (such as shading) for them to exist in an otherwise unfavorable climate. Because the dimensions of these valleys are below the 1-km topographic representation in the mass-balance model, we can resolve neither the topographic conditions favoring positive mass balance nor the small ablation areas (<1 km^2) associated with very negative mass-balance numbers.

Topographic features in the central Peruvian Andes cause a longitudinal precipitation gradient that ranges from >1200 mm year^{-1} in the east to 100 mm year^{-1} in the west (*26*). Low-resolution AGCMs cannot represent the topographic complexity of the region nor the associated precipitation gradients. To achieve realistic precipitation values for the PDD model, therefore, we used observed data from the Andes to derive a longitudinal gradient (*26*). The derived gradient results in a computed average ELA of 4870 m for the present, which agrees with the observed average value of 4900 m (Fig. 2). For the LGM simulations, precipitation anomalies (LGM minus control) simulated by GENESIS are applied to the derived gradient.

We reconstructed several LGM tropical glaciers by running the mass-balance model to obtain simulated areas that match those identified from moraines (*27*) (Fig. 3). Our model readily resolves the area of these glaciers, which were much larger and were less affected by local topographic controls than their modern counterparts; however, ELA gradients on Mauna Kea and Mt. Kilimanjaro that are dependent on local climate effects are not resolved. In New Guinea and Hawaii, where the OSU SST reconstruction is identical with that of CLIMAP, it was necessary to lower the LGM air temperatures from GENESIS by 2.0° to 3.4°C to achieve the targeted areas (Web table 1, available at www.sciencemag.org/cgi/content/full/290/5497/1747/DC1). In Africa, only slight temperature adjustments to the OSU simulation ($\leq$1°C) were needed, and no adjustments were needed over the Peruvian Andes, reflecting the effect of the regional cooling induced by the OSU SSTs.

The reconstructed LGM ELAs of all glaciers generally lie within 100 m of the estimates based on geologic evidence, and where modern glaciers exist for reference, the modeled LGM ELAs (relative to modern sea level) are ~800 to 870 m lower than at present (Web table 1 and Fig. 1). Baseline GENESIS

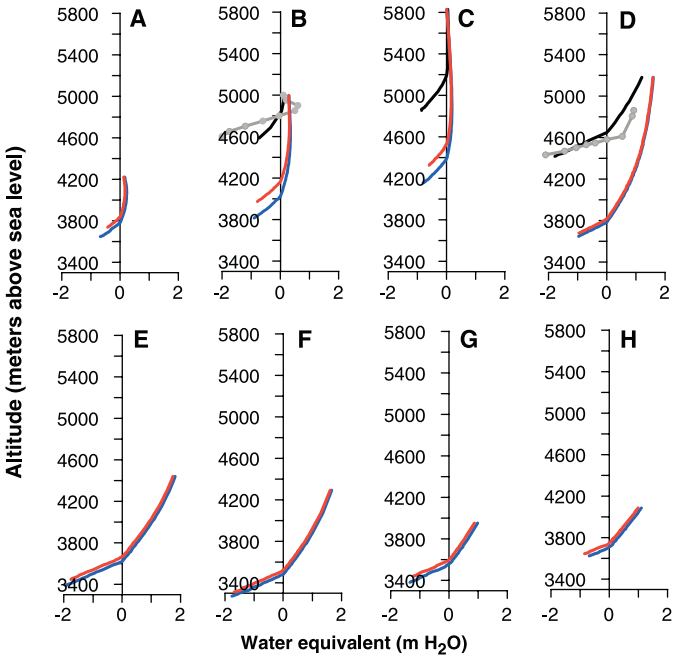

Fig. 1. Modeled mass-balance gradient curves for tropical glaciers as a function of meters water equivalent (mH_2O) and altitude. Positive values of mH_2O indicate the accumulation zone, and negative values indicate the ablation zone. ELA altitudes are located where the net balance is zero, and the elevation of the glacier terminus corresponds to the lowest elevation of the mass-balance values. The (upper) black curves are as simulated with the control (present) climatology, and the gray curves with symbols are observed mass-balance gradients. The lower curves are LGM mass balance as simulated with the OSU output (blue) and the CLIMAP output (red). (**A**) Mauna Kea, Hawaii. (**B**) Mt. Kenya, Africa; modern data from (*42*). (**C**) Mt. Kilimanjaro, Africa. (**D**) Irian Jaya, New Guinea; modern data from (*25*). (**E**) Mt. Wilhelm, Papua New Guinea (PNG). (**F**) Mt. Giluwe, PNG. (**G**) Mt. Albert Edward, PNG. (**H**) Saruwaged Range, PNG.

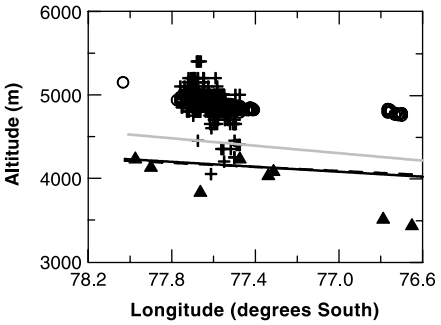

Fig. 2. Modeled ELAs as compared to observed ELAs for the Peruvian Andes along a longitudinal transect from 8.75°S to 9.25°S latitude, bracketing the latitude of the Huascarán ice core site [9.1°S (*23*)]. Computed control ELAs are represented by the open circles, and the observed modern ELAs (*31*) are represented by crosses. The solid triangles are the paleo-ELAs inferred from geologic data (*31*), the solid black line is a regression line fit to the ELAs simulated with the OSU output, and the gray line is a regression line fit to the ELAs as simulated with the CLIMAP output. The broken black line is a regression line fit to the ELAs simulated for 16 ka.

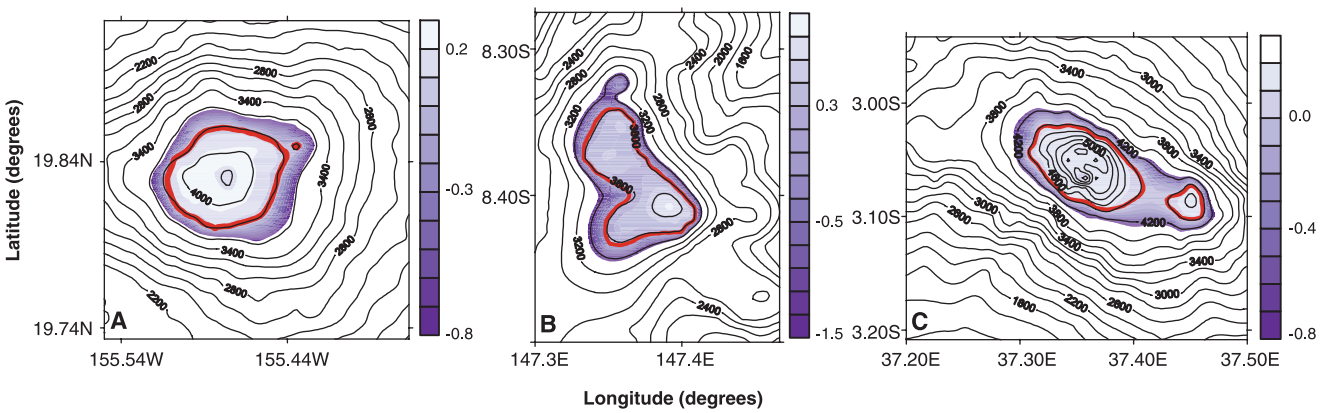

Fig. 3. Modeled glacier reconstructions for selected tropical glaciers obtained from the OSU output. Areal distributions of mass balance (in mH_2O) are overlaid on topographic maps derived from the 1-km data set. The position of the modeled ELA is indicated by the heavy red contour line. (**A**) Mauna Kea, Hawaii. (**B**) Mt. Albert Edward, PNG. (**C**) Mt. Kilimanjaro, Africa.

precipitation at the LGM ELAs ranges from 63% wetter than the control in Hawaii to 25% drier on Mt. Kenya, which is similar to changes inferred from pollen and lake-level data (Web table 1). At the LGM ELAs, mean annual air temperatures are from 3.5° to 6.6°C lower than control temperatures, indicating a range of overall tropical cooling consistent with that suggested by a number of proxies (*3*, *5*, *6*). In all locations, the amplitude of the seasonal cycle of air temperature is greater at the LGM than in the control simulation (*28*). Modeled changes in the temperature of the coldest month, a primary control of the altitudinal distribution of vegetation on tropical mountains, are in agreement with values inferred from pollen data (*5*) (Web table 1).

Temperature and precipitation values at the simulated ELAs of the New Guinea glaciers suggest that the eastern part of the island was generally drier and colder than the western part at the LGM. A tendency for west-to-east drying supports the hypothesis that the precipitation-bearing (easterly) trade winds were reduced (or eliminated) when emergent land replaced the Arafura Sea and Torres Strait during the low LGM sea level stand (*29*, *30*). An LGM reduction of up to ~50% in the strength of the easterlies in this region is simulated by GENESIS. Cooling in the east is consistent with an attendant reduced latent heating (evaporation) from the sea surface and increased sensible heating from the emergent land surface. The implied reduction of atmospheric vapor associated with these changes may have influenced LGM atmospheric lapse rates.

Based on geologic evidence, the average LGM ELA in the Peruvian Andes is 3950 m (range 3450 to 4250 m) (*31*), whereas the computed ELAs are 4170 (range 3750 to 4250 m) and 4440 m (range 4150 to 4440 m) with OSU and CLIMAP outputs, respectively (Fig. 2). The different ELAs produced by the OSU and CLIMAP outputs at the LGM reflect small temperature differences (OSU is ~2°C colder than CLIMAP at the Huascarán ice core site) and substantial precipitation differences (OSU is ~600 mm $year^{-1}$ wetter than CLIMAP at the Huascarán ice core site) between the GENESIS simulations. In agreement with the data, the PDD model displays a tendency for a west-to-east trend for lower LGM ELAs, which has been associated with enhanced advection from the Amazon basin (*31*), perhaps combined with changes in the surface energy balance due to attendant changes in cloudiness (*32, 33*). Again, as illustrated in the eastern part of the transect, the influence of complex topography on the climate of the region is not captured by the smoothed topographic representation of GENESIS.

Over Africa, the PDD model results indicate that the GENESIS simulation with the OSU SST reconstruction produces air temperatures at the ELA that support LGM glaciers at the sizes suggested by the geologic records. In contrast, the climatology produced by the CLIMAP SSTs at the OSU ELA is slightly warmer (~1°C), resulting in smaller glaciers with higher ELAs (Fig. 1).

Recent pollen-inferred estimates from low elevations (~460 m) on Hawaii suggest that LGM air temperatures were ~3°C lower and moisture levels were as much as ~30% less than at present (*34*). Our PDD model–derived temperature change of –3.5°C (Web table 1) agrees with the estimated cooling, but the modeled precipitation is greater than at present [which agrees with PMIP model simulations conducted with mixed-layer ocean models (*35*)]. A strong altitudinal gradient of precipitation associated with the tropical inversion exists in the tropics today. Changes in this gradient at the LGM could contribute to accommodating both moisture estimates. Alternatively, additional cooling of 1°C in the PDD model yields a glacier on Mauna Kea with precipitation values that are 33% less than at present. Our results from high elevations thus indicate that SSTs near Hawaii were ~2.5° to 3.5°C lower than those reconstructed by CLIMAP, a range of cooling comparable to that inferred by one recent reconstruction in the region (*36*).

The sensitivity and uniqueness of the modeled responses of the tropical glaciers are illustrated by plotting the glaciers in temperature-precipitation space (Fig. 4). Unlike high-latitude glaciers, the ELAs of the tropical glaciers are closely tied to the annual 0°C

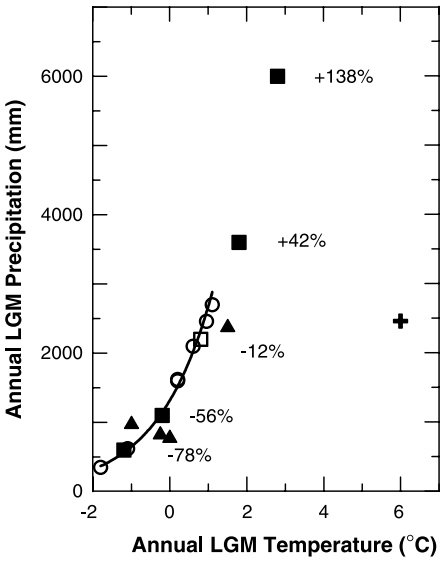

Fig. 4. Climate space of former tropical glaciers plotted as a function of annual LGM temperature and precipitation at the ELA. Open circles are the modeled glaciers, except for Mt. Giluwe, which is represented by the open square. The solid triangles represent modern tropical glaciers (*25*, *42–44*). For reference, the cross is the modern climate of Mt. Giluwe at the LGM ELA. Solid squares represent various prescribed perturbations of temperature and precipitation around the nominal LGM values that produce a glacier on Mt. Giluwe with the target area. The percentages associated with each Mt. Giluwe symbol are changes in annual precipitation relative to the GENESIS control values.

isotherm. As demonstrated by results for the LGM glacier on Mt. Giluwe, Papua New Guinea (PNG), lowering the nominal LGM temperature at the ELA thus requires substantial concomitant precipitation decreases to maintain the correct LGM area and ELA; raising that temperature requires concomitant precipitation increases (Fig. 4). Pollen data (*5*), however, indicate that maximum reductions of net moisture of ~30% relative to the present occurred in the vicinity of PNG at the LGM. Such a precipitation reduction could be accommodated by ~0.5°C of additional lowering of our nominal LGM temperatures. Any greater cooling would require unsupported precipitation decreases, whereas higher air temperatures would require increased precipitation, which conflicts with the pollen data. Reconciling the glacier model results with the pollen inferences thus constrains the range of LGM temperatures over Mt. Giluwe to be 6.6° to 7.1°C lower than at present. Similar arguments can be made for the other glaciers.

Uncertainties in the age control of late Pleistocene tropical glaciers gives rise to the long-standing question of whether tropical glacier advances were synchronous during the LGM, and thus whether observed ELA depressions reflect the climate of the LGM or that of some other period (*3*, *8–11*). To address this issue, we used output from a series of paleoclimate simulations for 21,000, 16,000, and 14,000 years ago (ka), conducted with Community Climate Model 1 (CCM1) (*37*) to scale LGM temperature and precipitation values in our PDD model. The sensitivity tests suggest that at 16 and 14 ka, warmer (~0.5° and 1.4°C, respectively) and wetter (1 and 1.7 mm day^{-1}, respectively) climatic conditions in the Peruvian Andes maintain modeled ELAs within 200 m of those at the LGM, which is consistent with observations that glaciers in the Peruvian Andes did not begin to retreat from the glacial maximum positions until ~14 ka (*38*). Glaciers similar to those of the LGM are also simulated in New Guinea under warmer (0.6°C) and wetter (2 mm day^{-1}) conditions at 16 ka. Post-LGM climatic conditions simulated by CCM1, however, are too warm and dry to support glaciers in Africa and too warm to support glaciers in Hawaii.

The climatology produced in GENESIS by the OSU SSTs results in ELAs and associated temperature and precipitation climatologies over Africa and the Andes that agree well with the geologic data, suggesting that the OSU SST reconstruction is sufficiently cool in the eastern Pacific and Atlantic Oceans. In the western Pacific Ocean, where the OSU and CLIMAP SSTs are the same, our glacier modeling supports the need for further cooling of the warm pool. Data analyses and climate model results (*3*, *6*, *34*, *39–41*) suggest that the warm pool was ~3.0°C colder than at present at the LGM (~2.0°C colder than CLIMAP). It is likely that these lower SSTs, possibly combined with modest increases in atmospheric lapse rates (*5*, *6*), induced the high-altitude cooling necessary to support glaciation on Hawaii and New Guinea. Apparent changes in LGM lapse rates, however, may be partly attributable to changes in the mean altitude of the base of the tropical inversion, which is determined by subsidence associated with the subtropical high-pressure cells (STHs), local and regional convection, and the trade winds. Although the inversion is not well resolved by lower resolution AGCMs, simulated LGM reductions in the strength of the STHs, coupled with changes in convection and the trade winds, support the possibility of increases in the mean altitude of the inversion base. Such an increase over Hawaii, for example, could result in substantially cooler and somewhat drier conditions at mid-altitude sites (1500 to 2000 m), together with greater precipitation at higher elevations, suggesting a need for understanding the role of the inversion in tropical climate change.

References and Notes

1. W. S. Broecker, G. H. Denton, *Geochim. Cosmochim Acta* **53**, 2465 (1989). ELAs, which separate the accumulation area from the ablation area on a glacier surface, are defined as the altitude where glacier mass balance equals zero. Although ELAs are sometimes used synonymously with snow lines, the two are not the same.
2. CLIMAP Members, *Geol. Soc. Am. Map Chart Ser.* **MC-3** (1981).
3. D. Rind, D. Peteet, *Quat. Res.* **24**, 1 (1985).
4. W. S. Broecker, *Global Biogeochem. Cyc.* **11**, 589 (1997).
5. I. Farrera *et al.*, *Clim. Dyn.* **15**, 823 (1999).
6. T. J. Crowley, *Clim. Dyn.* **16**, 241 (2000).
7. D. Joley, A. Haxeltine, *Science* **276**, 786 (1997); F. Street-Perrott *et al.*, *Science* **278**, 1422 (1997).
8. Ages are 15 to 20 ka for Huascarán [A. G. Klein, G. O. Seltzer, B. L. Isacks, *Quat. Sci. Rev.* **18**, 63 (1999)].
9. Ages are 10 to 30 ka for Kilimanjaro [C. Downie, P. Wilkinson, *The Geology of Kilimanjaro* (University of Sheffield, Sheffield, UK, 1972)].
10. Ages are <15 ka for New Guinea [E. Löffler, *Z. Geomorphol.* **13**, 32 (1972)].
11. Uncertainties are 9 to 22 ka for Hawaii [S. C. Porter, *Science* **195**, 61 (1977)].
12. A. C. Mix *et al.*, *Paleoceanography* **14**, 350 (1999).
13. S. W. Hostetler, A. C. Mix, *Nature* **399**, 673 (1999).
14. Boundary conditions include appropriate orbital geometry, atmospheric CO_2 concentration [340 parts per million by volume (ppmv) for control and 200 ppmv for LGM], prescribed continental ice sheets, and the Dorman and Sellers global vegetation data [J. L. Dorman, P. J. Sellers, *J. Appl. Meteorol.* **28**, 833 (1989)]. Each simulation was run for 15 years, and the first 4 years were excluded to allow the model to reach equilibrium.
15. Monthly average temperature and precipitation values at each grid point are computed by standard bilinear interpolation of the values from the nearest four GENESIS grid points. The temperatures of the glacier grid points are determined by vertical interpolation of temperature between the two GENESIS levels (altitudes) that bracket the altitude of the grid point.
16. The topography is represented by the GTOPO30 data set, a 30–arc sec (1-km) gridded elevation data set produced by the U.S. Geological Survey (available at http://edcdaac.usgs.gov/gtopo30/gtopo30.html).
17. T. Jóhannesson *et al.*, *J. Glaciol.* **41**, 345 (1994).
18. S. J. Marshall, G. K. C. Clarke, *Clim. Dyn.* **15**, 533 (1999).
19. D. Pollard, participating PMIP Members, *Global Planet. Change* **24**, 79 (2000).
20. Ablation and accumulation (the fraction of precipitation falling as snow) are computed in PDD models as parameterized functions of air temperature (which is a proxy for net radiation) and precipitation. Monthly temperatures are assumed to be normally distributed about the mean with specified Gaussian variance. To account for high levels of net radiation in the tropics, we specified the melting temperature of snow to be −1°C, instead of the value of 0°C or greater used for the high latitudes. The PDD model does not account explicitly for the radiation budget nor does it account for sublimation, which is a component of ablation in the high-altitude Andes.
21. H. Osmaston, in *Quaternary and Environmental Research on East African Mountains*, W. C. Mahaney, Ed. (Balkema, Rotterdam, Netherlands, 1989), pp. 31–104.
22. S. Hastenrath, L. Greischar, *J. Glaciol.* **43**, 455 (1997).
23. L. G. Thompson *et al.*, *Science* **269**, 46 (1995).
24. H. F. Diaz, N. E. Graham, *Nature* **383**, 152 (1996).
25. I. Allison, J. A. Peterson, in *The Equatorial Glaciers of New Guinea*, G. S. Hope *et al.*, Eds. (Balkema, Rotterdam, Netherlands, 1976), pp. 27–38.
26. J. A. J. Hoffman, *Climatic Atlas of South America* (World Meterological Organization, Geneva, Switzerland, 1975).
27. The LGM glaciers were constrained by estimates of maximum glacier areas estimated from the average positions of mapped moraine deposits. Because accumulation and ablation for the entire glacier are balanced in obtaining the best areal fits, the computations also yield the position of the ELA.
28. The greatest amplification is over the Andes (2°C LGM, 0.6°C control) and PNG (1.4°C LGM, 0.6°C control). LGM cooling over Hawaii is greater during the warmest months (5.4°C) than during the coldest months (−2.2°C).
29. H. A. Nix, J. D. Kalma, in *Bridge and Barrier: The Natural and Cultural History of Torres Strait*, D. Walker, Ed. (Publication BG/3, Department of Biogeography and Geomorphology, University of Australia, Canberra, Australia, 1972).
30. R. W. Galloway, G. S. Hope, E. Löffler, J. A. Peterson, in *Palaeoecology of Africa and Antarctica*, E. M. van Zinderen Bakker, Ed. (Balkema, Cape Town, South Africa, 1973), vol. 8, pp. 125–138.
31. This elevation is derived from the raw data provided courtesy of A. Klein, originally published in A. G. Klein, G. O. Seltzer, B. L. Isacks, *Quat. Sci. Rev.* **18**, 63 (1999).
32. S. Hastenrath, A. Ames, *J. Geophys. Res.* **100**, 5105 (1995).
33. G. Kaser, C. Georges, *Ann. Glaciol.* **24**, 344 (1997).
34. S. Hotchkiss, J. O. Juvik, *Quat. Res.* **52**, 115 (1999).
35. S. Pinot *et al.*, *Clim. Dyn.* **15**, 857 (1999).
36. K. E. Lee, N. C. Slowey, *Nature* **397**, 512 (1999).
37. J. E. Kutzbach *et al.*, *Quat. Sci. Rev.* **17**, 473 (1999). The sensitivity tests were performed by appending CCM1 temperature and precipitation anomalies (21 ka minus 16 ka and 21 ka minus 14 ka) to the 21-ka OSU GENESIS simulation.
38. G. O. Seltzer, *Quat. Sci. Rev.* **9**, 137 (1990).
39. A. Ganopolski, S. Rahmstorf, V. Petoukhov, M. Claussen, *Nature* **391**, 351 (1998).
40. A. J. Weaver, M. Eby, A. F. Fanning, E. C. Wiebe, *Nature* **394**, 847 (1998).
41. D. W. Lea, D. K. Pak, H. J. Spero, *Science* **289**, 1719 (2000).
42. S. Hastenrath, *The Glaciers of Equatorial East Africa* (Reidel, Dordrecht, Netherlands, 1984).
43. P. Wagnon, P. Ribstein, G. Kaser, P. Berton, *Global Planet. Change* **22**, 49 (1999).
44. L. G. Thompson, E. Mosley-Thompson, P. Grootes, N. Pourchet, *J. Geophys. Res.* **89**, 4638 (1984).

45. We thank P. Bartlein, A. Mix, D. Pollard, and D. Zahnle for discussions and reviews. Supported by the U.S. Geological Survey and the Earth Systems History Program of NSF.

20 July 2000; accepted 13 October 2000